Electrochimica Acta 571 (2026) 149030

Contents lists available at ScienceDirect

Electrochimica Acta

journal homepage: www.journals.elsevier.com/electrochimica-acta

The effect of zinc and acetate species on the corrosion behaviour of steels

R. Addai [a,d], S. Ramamurthy [b], D. Zagidulin [a], Z. Wang [a], C. Power [c], J.M.C. Mol [d], Y.S. Hedberg [a,b,d,*]

[a] Department of Chemistry, The University of Western Ontario, London, Ontario, N6A 5B7, Canada
[b] Surface Science Western, The University of Western Ontario, London, Ontario, N6G 0J3, Canada
[c] Department of Civil and Environmental Engineering, The University of Western Ontario, London, Ontario, Canada
[d] Department of Material Science and Engineering, University of Delft Technology, Delft, the Netherlands

ARTICLE INFO

Keywords:
Atmospheric corrosion
De-icer
Complexation
Electrochemistry
Solubility

ABSTRACT

De-icing road salts are widely employed for snow and ice mitigation in cold climate regions, with sodium chloride (NaCl) being the most commonly used salt. The extensive application of NaCl has raised significant infrastructure, sustainability, and environmental concerns, and it has led to the emergence of various alternative de-icing salts, including other chloride-based and organic salts and compounds. In this study, the effect of zinc and acetate species on the corrosion behaviour of steels was systematically investigated using a combination of atmospheric corrosion testing, immersion testing, electrochemical measurements, cross-sectional microscopy, Zn K-edge X-ray absorption spectroscopy (XANES), and thermodynamic speciation modelling. The effect of eight chloride and non-chloride salts and their mixtures on the corrosion of structurally important galvanized steel, mild steel, and high-strength steel was studied. The chloride-based salts were found to be more detrimental than the organic salts to the corrosion of mild and high-strength steels, but all the salts were similarly corrosive to galvanized steel. It was found that the presence of both zinc and acetate species significantly enhanced corrosion and the Fe dissolution rate in steels. >40 wt.% of the 20 μm-thick galvanized zinc layer was dissolved after one week of immersion in 0.5 M sodium chloride or sodium acetate. After this one-week immersion, or the 10-week atmospheric field exposure, any remaining zinc was entirely in the form of zinc oxide. Our findings call for further investigation before using organic de-icing salts, alone or in mixtures with NaCl, on galvanized steel.

1. Introduction

De-icing road salts are extensively used for snow and ice control during winter in cold climate regions. Upon application to the road surface, the de-icing salts melt the ice and form a salt brine that has a freezing point below zero [1]. For example, sodium chloride (NaCl) can lower the freezing point of water to as low as –21 °C [2,3]. NaCl has long been the most commonly applied salt due to its low-cost and broad availability [4]. However, its widespread application has raised significant concerns about its effects on transportation, infrastructure, and the environment [5]. This has led to the emergence of alternative de-icing salts, including other chloride-based salts, such as potassium chloride (KCl), magnesium chloride ($MgCl_2$), and calcium chloride ($CaCl_2$) [6], organic salts or substances, including formate-based and acetate-based salts, such as calcium magnesium acetate (CMA) and sodium acetate (NaOAc), beet root juice, sugars, and other natural products [7].

Among commonly used structural materials, carbon and low-alloy steels remain particularly susceptible to corrosion in chloride-containing environments, where the breakdown of passive films and enhanced anodic dissolution dominate degradation processes [8,9].

Metal corrosion in atmospheric environments, particularly in the presence of road de-icing salts, is a critical factor that influences the durability and performance of infrastructure materials [10,11]. Low-alloyed steels, galvanized steel (GS), stainless steels, and aluminum alloys are metals that are widely employed in infrastructure and automotive industries due to their mechanical strength and corrosion resistance [12–14]. Among these, GS is widely employed to mitigate corrosion of steels through the sacrificial action of a zinc coating. Zinc provides cathodic protection to the underlying steel substrate and typically forms corrosion products such as zinc oxide (ZnO), zinc hydroxide ($Zn(OH)_2$), or zinc carbonate ($ZnCO_3$, in atmospheric conditions), that can impart partial barrier protection under atmospheric

* Corresponding author at: Department Chemistry, The University of Western Ontario, London, Ontario, N6A 5B7, Canada.
E-mail addresses: raddai2@uwo.ca (R. Addai), sramamur@uwo.ca (S. Ramamurthy), dzagidul@uwo.ca (D. Zagidulin), zwang443@uwo.ca (Z. Wang), cpower24@uwo.ca (C. Power), J.M.C.Mol@tudelft.nl (J.M.C. Mol), yhedberg@uwo.ca (Y.S. Hedberg).

https://doi.org/10.1016/j.electacta.2026.149030
Received 21 January 2026; Received in revised form 20 April 2026; Accepted 4 May 2026
Available online 6 May 2026

exposure [15,16]. The electrochemical behaviour of zinc coatings in chloride-containing electrolytes has been extensively studied, with particular emphasis on anodic dissolution kinetics, corrosion product formation, and the stability of zinc hydroxychloride phases [17,18].

However, less attention has been devoted to zinc behaviour in acetate-containing environments, despite the increasing use of acetate-based de-icing salts and the growing environmental shift toward chloride alternatives [19,20]. Acetate ions are known to act as complexing ligands for the zinc ion (Zn^{2+}), forming soluble zinc–acetate species whose stability depends strongly on pH and concentration [21]. Such complexation can increase zinc solubility and potentially suppress the precipitation of protective $Zn(OH)_2$, ZnO, or $ZnCO_3$ [22]. However, the consequences of these processes for the corrosion of zinc-coated steels and for steels exposed to dissolved zinc species remain insufficiently resolved. Previous corrosion studies of acetate-based de-icing salts have largely focused on comparative corrosion rates relative to chlorides, often reporting lower aggressiveness toward carbon steels [23]. Nevertheless, emerging observations suggest that GS steels may not follow the same trend, indicating that the interaction between dissolved zinc species and acetate-containing electrolytes may introduce additional mechanistic complexity [20,23]. In particular, the role of soluble Zn–acetate complexes in destabilizing the sacrificial protection mechanism and accelerating substrate exposure has not been systematically investigated. Mild steel (MS) and high-strength steel (HS) are among the most widely used structural alloys due to their low cost, ease of fabrication, and favourable mechanical properties [24,25]. While MS and HS are evaluated on mechanical performance, the utility of GS is entirely dependent on the integrity of the zinc-electrolyte interface. In standard atmospheric testing, GS is expected to outperform bare MS/HS by a factor of 20 to 40 [26]. However, less information is reported under aggressive or prolonged exposure of GS to certain deicing salts; the traditional "protection factor" of GS may diminish.

The objective of this study was to investigate the effect of acetate salts, inspired by our study on different de-icer salts, on the corrosion susceptibility of GS compared to steels without zinc. A suite of field and laboratory corrosion tests was conducted under various atmospheric and aqueous conditions and supported by an array of material, surface, solution analytical, and speciation modelling tools. The findings provide new mechanistic insight into how zinc acetate complexation not only destabilizes the zinc layer but also accelerates the corrosion of the underlying steel, challenging the common assumption that acetate-based salts are benign alternatives to chlorides [27].

2. Materials and methods

2.1. Metals, salts, and sample preparation

Ferritic and martensitic GS (hot-dip galvanized), ferritic MS, and martensitic HS sheets (1 mm thick) were obtained from SSAB AB (Borlänge, Sweden). Table 1 presents the nominal bulk alloy composition for each metal as provided by the supplier.

The sheets for each metal were shear-cut into square pieces, with 50 mm × 50 mm pieces required for the atmospheric corrosion field tests, and 10 mm × 10 mm pieces used in the electrochemical and immersion laboratory tests. For atmospheric corrosion, electrochemical, and immersion tests, GS sheets were used in their as-received surface states, whereas MS and HS metal coupons were ground (as described below) for all experimental testing. The metal coupons were ground using a series of silicon carbide (SiC) grinding papers down to grit P1200 and deionized (DI) water as a lubricant, to achieve a similar starting surface condition. The coupons were then ultrasonically cleaned in acetone and ethanol for 5 min each and dried with nitrogen gas at room temperature.

Table 1
Nominal bulk alloy composition of the metal coupons (wt %) (per supplier information). Other information on the manufacturing process and mechanical properties is indicated in the footnotes.

Name	Galvanized steel (substrate)	Mild steel	High-strength steel
Short name	GS[a]	MS[b]	HS[c]
Fe	balance	balance	balance
Al	0.885	0.036	0.045
C	0.107	0.053	0.14
Cr	0.046	0.038	0.027
Ni	0.033	0.051	0.037
Mn	1.72	0.22	1.5
S	0.0006	0.0044	0.0029
N	0.0036	0.0031	0.0031
P	0.01	0.003	0.009
Si	0.363	0.005	0.199
Mo	0.007	0.012	0.002
Nb	0.004	0.001	0
V	0.007	0.002	0.01
Ti	0.006	0.001	0.035
B	0.001	0.0011	0.0017
Cu	0.015	0.02	0.148

[a] dual-phase (ferrite and martensite) steel with small amounts of bainite and retained austenite. Hot-dip metal coated with zinc (>99 %). Yield strength $R_{p0.2}$ 405 MPa, tensile strength R_m 637 MPa, A80 28 %.
[b] cold-rolled ferritic steel. Yield strength $R_{p0.2}$ 207 MPa, tensile strength R_m 334 MPa, A80 41 %.
[c] cold-rolled martensitic steel. Yield strength $R_{p0.2}$ 1194 MPa, tensile strength R_m 1405 MPa, A80 4 %.

After the grinding and cleaning, and prior to any testing, all coupons were stored in a desiccator (relative humidity <10 %) at room temperature for 24 ± 1 h. This preparation procedure ensured reproducible surface oxide growth and comparison with other studies [28].

Eight of the most common alternative de-icing salts were selected for this study, as summarized in Table 2. The chloride-based salts consist of NaCl, KCl, $MgCl_2$, and $CaCl_2$, with a second NaCl salt (NaCl+tr) being the salt used by Facilities Management on the campus of Western University and known to contain traces of organic salts and impurities. The organic salts in this study consisted of CMA, which is NaCl enriched with ≤10 % CMA, NaOAc, and chloride-free blend (CFB), which is a chloride-free, proprietary salt provided by Cypher Environmental Ltd. Additionally, zinc acetate ($Zn(OAc)_2$) salt (analytical grade, Millipore Sigma, Canada) was selected as a reference salt to study the hypothesis whether both zinc and acetate ions are needed to accelerate the corrosion of steel.

2.2. Solution preparation

The salt brine solutions used in this study were prepared from the salts (Table 2) and Type I (ultrapure) water (18.2 MΩ cm resistivity) obtained from a Milli-Q Reference system (Millipore Sigma, Canada). All flasks, test tubes, and glassware used in this study were thoroughly cleaned using a 10 % nitric acid (analytical grade) bath at room temperature for a minimum of 24 h to ensure no contamination, especially for the trace metal analysis. After acid cleaning, the glassware was rinsed at least four times with ultrapure water. Three distinct concentrations of salt solutions were prepared for the different tests in this study: (*i*) 100 g/L solutions for atmospheric corrosion studies, (*ii*) 0.5 M solutions for immersion tests, and (*iii*) 0.1 M solutions for electrochemical experiments at their respective natural pH values. Constant mass concentrations among the road salts were necessary as de-icing applicators work with mass concentrations, but to enable chemical insights, we also investigated the salts at similar molar concentrations, using the molecular masses reported in Table 2.

Table 2
List of the eight de-icing salts used in this study.

Name	Abbreviation	Considered molecular mass (g/mol)	Grade	Supplier
Sodium chloride	NaCl	58.44	Commercial (unknown impurities)	Cypher Environmental Ltd. (Canada)
Potassium chloride	KCl	74.55	Analytical	Millipore Sigma (Canada)
Magnesium chloride	$MgCl_2$	95.21	Analytical	Millipore Sigma (Canada)
Calcium chloride	$CaCl_2$	110.98	Commercial (unknown impurities)	Cypher Environmental Ltd. (Canada)
Sodium chloride + calcium magnesium acetate	CMA	75.85 (95 % of 58.44 + 5 % of 406.59)	Commercial (unknown impurities)	Snow Joe (USA)
Sodium chloride + trace impurities	NaCl+tr	58.44	Commercial (unknown impurities)	Western University (Canada)
Sodium acetate	NaOAc	82.03	Analytical	Millipore Sigma (Canada)
Chloride-free blend	CFB	proprietary	Commercial (unknown impurities)	Cypher Environmental Ltd. (Canada)

2.3. Experimental atmospheric corrosion field tests

Field tests were conducted at the field site (at the campus of Western University, 43°00′56.6″N 81°16′57.3″W), where the metal coupons were exposed to the different salts during the 2022 winter season (January 26 to April 13). Over the testing period, daily air temperature ranged from –16.9 °C to 25.4 °C, with a mean of 0.1 °C. Maximum daily precipitation reached 28.1 mm, with an average of 2.4 mm, while snow on the ground reached a maximum depth of 21.1 cm, with a mean of 5.8 cm (Environment Canada, 2026). Temporal variations in daily air temperature, precipitation, and snow cover are shown in **Fig. S1** in the Supporting Information.

Eight triangular-shaped prism fixtures used to hold the metal coupons in place during the field tests were fabricated by University Machine Services at Western University. Each fixture was made from polymethyl methacrylate (Plexiglass), measuring 60 cm in length, 7 cm in width, and 7 cm in height, and with a surface inclination of 45° (**Fig. S2**) [29]. Prior to the field tests, all metal coupons (each metal type in triplicate; 15 in total; including stainless steel 304 and aluminum alloy) were weighed using an analytical balance (accuracy: 0.1 mg) and then securely mounted on each of the eight Plexiglass fixtures using plastic screws and fasteners to prevent galvanic corrosion, with extra care taken to avoid cross-contamination of salts (details in **Section S2** in Supporting Information).

Eight general-use 1 L plastic sprayers were used to apply the salt solutions to the metal coupons. Each sprayer was filled with a 100 g/L salt solution of the respective salt, and approximately 12 mL of the solution was sprayed on each of the 15 metal coupons (*e.g.*, NaCl solution was applied to each of the five metals, in triplicate, on its corresponding Plexiglass fixture). Salt application occurred once a week over the field test duration of 10 weeks, with photographs taken of each metal coupon to document the metal surface changes over time. At the end of the field test, the metal coupons were carefully removed from the Plexiglass and placed in a vacuum desiccator for a minimum of 24 h to ensure that they were stabilized and moisture-free before further analysis, including mass loss measurements and surface analyses. All tests were conducted on triplicate samples of metal coupons to ensure data reproducibility and consistency.

2.4. Immersion tests

Immersion tests were performed by immersing the metal coupons within each respective salt solution over two exposure durations: 24 and 168 h. Each coupon was placed in a vertical upright position and immersed in 4 mL of salt solution inside a 5 mL acid-cleaned plastic vial. Both sides of the coupon were exposed to provide an exposed geometrical surface area of 2.2 cm^2, which corresponds to a 0.55 cm^2/mL surface area to solution ratio. A blank sample (without any metal coupon) was included as a control for each set of triplicate samples. The vials were then placed inside an incubating orbital shaker (VWR, Canada) that was set to operate at 80 rpm at room temperature and under attenuated light conditions.

At the end of each exposure period, the coupons were removed from the solutions and rinsed with 1 mL of Type I water. The rinsed water was collected and added to the corresponding solution. The solutions, including the blanks, were acidified using ultrapure 65 % nitric acid (HNO_3) to achieve a pH < 2. The acidified solutions were stored at room temperature until further analysis was conducted. Before mass loss measurements and surface analyses, the coupons were dried with nitrogen gas at room temperature and stored in a vacuum desiccator to prevent contamination and moisture interference.

2.5. Inductively coupled plasma mass spectrometry (ICP-MS)

The amounts of trace metals released from the metal samples (GS, MS, HS) during exposure to the 0.5 M salt solutions were measured using inductively coupled plasma mass spectrometry (ICP-MS) with an iCAP Q instrument (Thermo Fisher, Canada). For this analysis, only the concentrations of specific metals – iron (Fe), zinc (Zn), chromium (Cr), manganese (Mn), and nickel (Ni) – were measured. The metal concentrations within the corresponding blank solutions (c_{blank}), if detectable, were subtracted from the sample concentrations (c_{sample}). The limits of detection, as determined from the background levels and the instrument's detection limit, were 2.18, 0.97, 0.06, 0.16, and 0.13 µg/L for Fe, Zn, Mn, Cr, and Ni, respectively. All calibration curves were linear ($R^2 > 0.9993$) based on blank and standard concentrations (in 2 % HNO_3) up to 320, 300, 250, 240, and 240 µg/L for Fe, Zn, Mn, Cr, and Ni, respectively. Spiked blank samples were run throughout the analyses, and the criterion for re-analysis was a recovery of <80 % or >120 %.

Eq. (1) was used to calculate the amounts of trace metal released (in

μg/cm^2). The exposure volume, *V*, was 0.004 L for all salt solutions. The surface area, *A* (2.2 cm^2), was the geometrically exposed surface area of the exposed coupon. The dilution factor (*DF*) is the unitless factor determined from the final volume divided by the initial solution sample volume.

$$\textit{Amount of metal released}\ \left(\mu g/cm^2\right) = \frac{\left(c_{sample}\left(\frac{\mu g}{L}\right) - c_{blank}\left(\frac{\mu g}{L}\right)\right) \times DF_{sample} \times V\ (L)}{A\ (cm^2)} \quad (1)$$

2.6. Mass loss determination

2.6.1. Pickling

Following the analytical measurements of metals exposed to both the field exposure and immersion tests, a chemical pickling process was employed to remove corrosion products with minimal impact on the base metal. The pickling process was performed based on the following sections in the American Society for Testing and Materials (ASTM) standards [30]: C9.5 for GS and C3.5 for MS and HS.

2.6.2. Mass loss

To evaluate the mass loss from the metal coupon due to corrosion after the field exposure or the one-week immersion, a three-step mass measurement protocol was employed: (*i*) the initial mass (m_1) of each coupon was recorded prior to exposure in the field test (10 weeks) and immersion tests (1 week), (*ii*) the dried coupons were carefully weighed after the exposure period to document any weight changes (gain or loss) caused by corrosion or deposition of corrosion products (m_2), and (*iii*) the coupons were weighed a final time (m_3) after undergoing the chemical pickling process, reflecting the sample mass after the removal of corrosion products. The differences between m_1 and m_3 were used to quantify mass loss using Eq. (2):

$$\textit{Mass loss}\ \left(\frac{\mu g}{cm^2}\right) = \frac{\Delta m\ (g)\ x\ 10^6}{A\ (cm^2)} \quad (2)$$

Where Δm is the difference between the initial mass and the final mass (m_1 - m_3) in grams, and *A* is the exposed geometrical surface area of the coupon (cm^2). The use of m_2 is specified in Section 2.13.

2.7. Cross-sectional analysis

For cross-sectional analysis, as-received (unexposed) GS and GS exposed to 168 h 0.5 M NaCl and NaOAc solutions were mounted in epoxy resin and ground by P4000 SiC paper to obtain a flat and representative cross-section of the zinc coating and underlying steel substrate. The zinc or zinc oxide thickness was determined from scanning electron microscopy (SEM) cross-sectional images by multiple measurements (4 locations with 5 measurements each) across different regions of each sample. The average values and corresponding standard deviations were used to quantify the initial Zn layer thickness and its reduction after the immersion exposure.

Elemental distributions across the cross-sections were analysed using energy-dispersive X-ray spectroscopy (EDX) mapping to assess changes in Zn distribution, corrosion product formation, and the exposure of the underlying steel substrate.

2.8. Optical and scanning electron microscopy (OM and SEM)

The surface morphology of the metal coupons was examined before and after pickling, as well as before and after exposure in the field and immersion tests, to evaluate changes in surface characteristics. Optical surface observations were performed using a Keyence VHX-6000 digital optical microscope. Additional surface analysis and the cross-sectional analysis described in Section 2.7 were conducted using a Hitachi SU3900 variable pressure SEM equipped with an Oxford ULTIM MAX 65 SDD X-ray detector for EDX. The SEM was operated at an accelerating voltage of 10–15 kV.

2.9. X-ray absorption near-edge structure (XANES) spectroscopy

Zn K-edge X-ray absorption near-edge structure (XANES) spectroscopies of the unexposed GS coupon and exposed coupons after the 168 h immersion tests in NaCl and NaOAc were collected on the I18 beamline of the Diamond Light Source, United Kingdom. The beamline energy was calibrated using zinc foil as a reference ($E_0 = 9659$ eV). The fluorescence yield (FY) spectrum was recorded by a vortex Si drift detector and normalized to the incident photon flux (I_0). XANES was collected from three spots on each sample. XANES of ZnO, $Zn(CH_3COO)_2$ and $ZnCl_2$ reference materials (all analytical grade) were also measured as a reference. The Zn K-edge XANES spectra were processed using Athena software (version 0.9.26) [31].

2.10. Electrochemical measurements

Electrochemical measurements were performed using a BioLogic VSP-300 potentiostat/galvanostat controlled by EC-Lab v11.60 software or a Modulab XM ECS system (AMETEK Solartron Analytical, Oak Ridge, TN, USA). A three-electrode setup with a flat cell at room temperature was used that comprised: (*i*) saturated (KCl) Ag/AgCl electrode as the reference electrode (–197 mV *vs.* standard hydrogen electrode), (*ii*) platinum mesh as the counter electrode, and (*iii*) any of the three metal samples (GS, MS, and HS) with an exposed geometrical surface area of 0.785 cm^2, controlled by an O-ring inner diameter, as the working electrodes. All potentials are indicated *versus* $Ag/AgCl_{(sat.)}$ unless otherwise specified. The working electrodes were immersed in their respective salt solutions for 1 h to establish a steady-state open circuit potential (OCP) before applying other electrochemical testing techniques. Linear polarization resistance (LPR) measurements were conducted within ±15 mV *versus* OCP at a scan rate of 0.5 mV/s to assess the polarization resistance. For potentiodynamic polarization tests, the potential was swept from –0.25 V to 1 V *versus* OCP at a scan rate of 0.5 mV/s to determine the corrosion current density and the corrosion potential.

2.11. Thermodynamic speciation modelling

To determine the predominant equilibrium species and corrosion products, the Joint Expert Speciation System (JESS, version 8.8 v) was used [32–34]. All input values, which were based on the conditions of the immersion and field tests, are described in **Table S1** in **Section S3** in the Supporting Information. Between 98 and 235 (electro)chemical reactions were considered for each condition. Solids were allowed to form

and precipitate, allowing for the determination of predominant corrosion products and their equilibrium solubility. The equation-solving algorithm was damped Newton-Raphson with a maximum of 200 iterations and a maximum delta[log(unknown)] of 2.0. The convergence criterion was either that the sum of absolute equation values was <0.04 or that each delta[log(unknown)] was <0.0001. All coding, conditions, and all included and omitted reactions for each element and salt can be found in the associated dataset (see **Data Availability Statement**).

2.12. Statistical analysis

A Student's *t*-test for unequal variance and unpaired data was used to compare two different datasets of independent samples for two different conditions. If the probability (p) of these datasets being equal was smaller than 0.05, it was deemed to be a statistically significant difference. For calculations, the software KaleidaGraph v.4.0 (Synergy Software, US) was used.

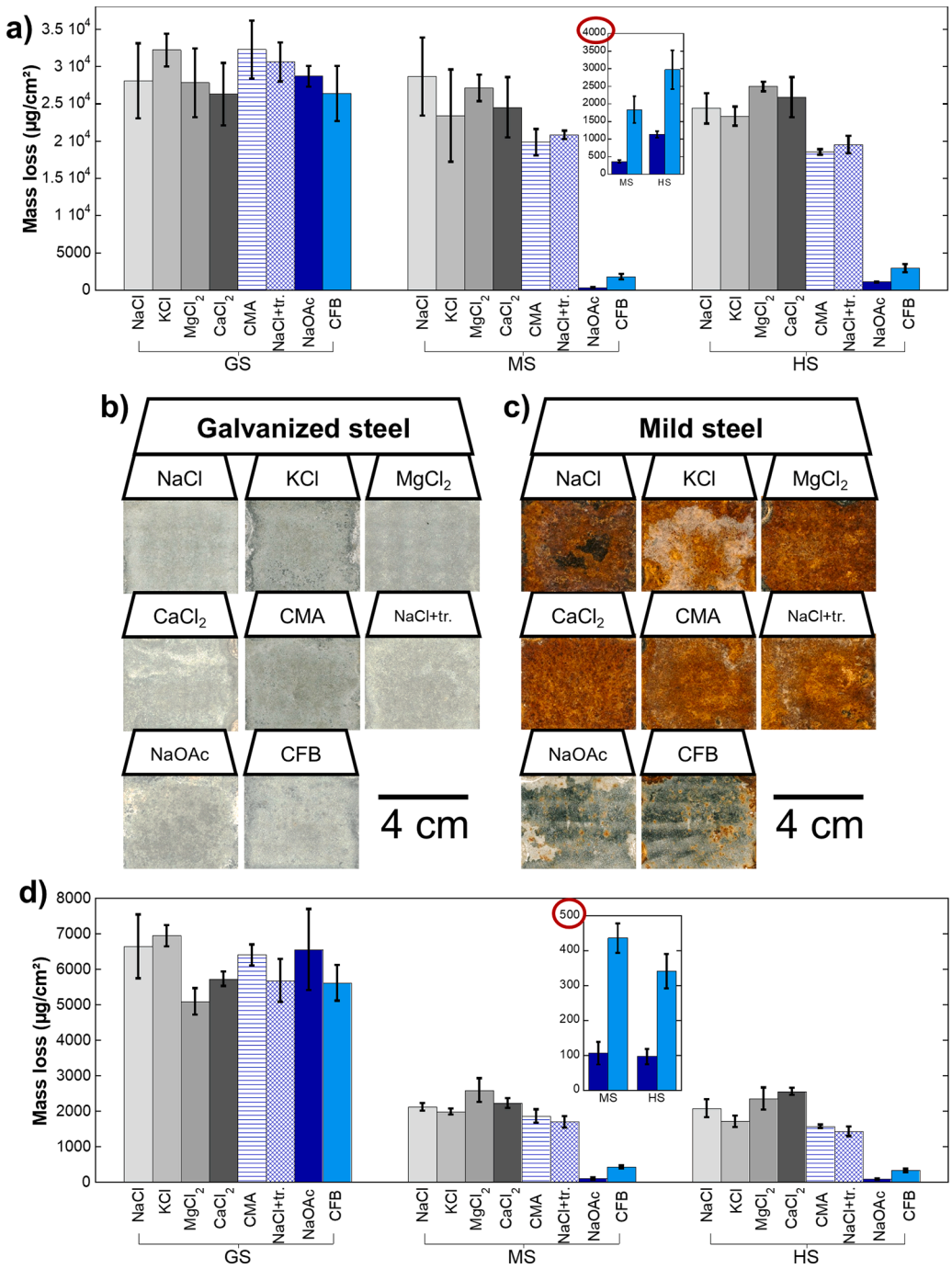

Fig. 1. Mass loss and corresponding OM images of GS, MS, and HS after exposure to the eight road de-icing salts (0.1 g/L once sprayed per week) for 10 weeks of winter exposure in the field tests: (a) mass loss of GS, MS, and HS (b) optical microscopy images of GS surfaces, (c) optical microscopy of MS, and (d); mass loss of immersion tests of GS, MS, and HS in 0.5 M salt solutions for 168 h at 25 °C. The error bars indicate the standard deviation of triplicate coupons. CMA denotes 95 wt. % NaCl + 5 wt. % CMA.

2.13. Calculation of Zn layer reduction and mass loss across different techniques

To quantify and validate mass loss and corrosion products across different techniques for unexposed GS and GS exposed to 0.5 M NaCl or 0.5 M NaOAc for 168 h (immersion), the following calculations were conducted. The mass loss of Zn in wt. % of the total available Zn was estimated from the mass loss (Eq. (2)) and converted to wt. % by Eq. (3). Zn mass loss in wt. % of the total available Zn was further estimated by the XANES edge jump (E.J.) as described in Eq. (4).

$$\textit{Mass loss}\ (\text{wt.\%}) = \frac{\text{mass loss}\left(\frac{\text{g}}{\text{cm}^2}\right)}{\delta_{\text{Zn}}\left(\frac{\text{g}}{\text{cm}^3}\right) \times \text{d}\ (\text{cm})} \times 100\ wt.\% \tag{3}$$

$$\textit{Mass loss}\ (\text{wt.\%}) = \frac{\left(\text{E.J.}_{\text{unexposed}} - \text{E.J.}_{\text{exposed}}\right)}{\text{E.J.}_{\text{unexposed}}} \times 100 wt.\% \tag{4}$$

Where δ_{Zn} is 7.14 g/cm^3 and d is the measured (by cross-section, Section 2.7) initial Zn layer thickness of the unexposed GS (0.0020247 cm). The remaining Zn layer for the exposed GS samples (to either NaCl or NaOAc) was assumed to be 100 % ZnO in these calculations, based on the findings by XANES (Section 3.2). Further, the remaining (after the 168 h immersion) ZnO thickness was measured by cross-section analysis (Section 2.7) and compared to estimated ZnO thicknesses by XANES (Eq. (5)) and mass loss and mass gain measurements (Eq. (6)).

$$\textit{Thickness of ZnO}\ (\mu\text{m}) = \frac{(100 - \text{mass loss (Eq.4)}) \times \delta_{\text{Zn}}\left(\frac{\text{g}}{\text{cm}^3}\right) \times \text{M}_{\text{ZnO}}\left(\frac{\text{g}}{\text{mol}}\right) \times \text{d}\ (\mu\text{m})}{100 \times \delta_{\text{ZnO}}\left(\frac{\text{g}}{\text{cm}^3}\right) \times \text{M}_{\text{Zn}}\left(\frac{\text{g}}{\text{mol}}\right)} \tag{5}$$

$$\textit{Thickness of ZnO}(\mu\text{m}) = \frac{\text{m}_2(\text{g}) - \text{m}_3(\text{g})}{\text{cm}^2 \times \delta_{\text{ZnO}}\left(\frac{\text{g}}{\text{cm}^3}\right)} \times 10,000 \tag{6}$$

Where δ_{ZnO} is 5.61 g/cm^3, M_{ZnO} is 81.4 g/mol, M_{Zn} is 65.4 g/mol, and m_2 and m_3 are the masses measured after exposure and after the removal of the corrosion products (Section 2.6.2). Finally, the fractions of the corroded Zn from GS exposed to 0.5 M NaCl or 0.5 M NaOAc for 168 h transitioning into the aqueous phase (Zn_{aq}) and into the solid phase (as ZnO, Zn_s) were estimated from the ICP-MS measurements (Eq. (1) converted into wt. % by Eq. (7)) for the aqueous phase, and from XANES (Eq. (8)), the cross-sectional analysis (Eq. (9)), and mass loss measurements (Eq. (10)) for the solid phase.

$$\text{Zn}_{\text{aq}}\ (\text{wt.\%}) = \frac{\text{Zn release}\left(\frac{\mu\text{g}}{\text{cm}^2}\right)}{1,000,000 \times \delta_{\text{Zn}}\left(\frac{\text{g}}{\text{cm}^3}\right) \times \text{d}\ (\text{cm})} \times 100\ wt.\% \tag{7}$$

$$\text{Zn}_{\text{s}}\ (\text{wt.\%}) = \frac{\text{Thickness of ZnO}\ (\mu\text{m},\ \text{Eq.5}) \times \delta_{\text{ZnO}}\left(\frac{\text{g}}{\text{cm}^3}\right)}{10,000 \times \delta_{\text{Zn}}\left(\frac{\text{g}}{\text{cm}^3}\right) \times \text{d}\ (\text{cm})} \times 100\ wt.\% \tag{8}$$

$$\text{Zn}_{\text{s}}\ (\text{wt.\%}) = \frac{\text{d}_{\text{ZnO}}\ (\mu m) \times \delta_{\text{ZnO}}\left(\frac{\text{g}}{\text{cm}^3}\right)}{10,000 \times \delta_{\text{Zn}}\left(\frac{\text{g}}{\text{cm}^3}\right) \times \text{d}\ (\text{cm})} \times 100\ wt.\% \tag{9}$$

$$\text{Zn}_{\text{s}}\ (\text{wt.\%}) = \frac{\text{Thickness of ZnO}\ (\mu\text{m},\ \text{Eq.6}) \times \delta_{\text{ZnO}}\left(\frac{\text{g}}{\text{cm}^3}\right)}{10,000 \times \delta_{\text{Zn}}\left(\frac{\text{g}}{\text{cm}^3}\right) \times \text{d}\ (\text{cm})} \times 100\ wt.\% \tag{10}$$

Where d_{ZnO} is the measured (by cross-section analysis) ZnO layer thickness on the GS after exposure to 0.5 M NaCl or 0.5 M NaOAc for 168 h.

3. Results and discussion

3.1. Atmospheric and immersion exposures

Fig. 1a–c present mass loss data and corresponding optical images of the GS, MS, and HS samples after 10 weeks of atmospheric field exposure with different salt types (sprayed once a week with 0.1 g/L salt brines). Fig. 1d presents the corresponding mass loss data after one week of immersion in 0.5 M of these salt solutions (with corresponding corrosion rates in **Table S4** in **section S4**). In atmospheric conditions, all three steel types, GS, MS, and HS, exhibited mass loss of 20 to 30 mg/cm^2 when exposed to chloride-based salts. Those mass losses were much higher than those in the pure organic salts (NaOAc, CFB: 0.3–3 mg/cm^2) for MS and HS, but not GS. The level of corrosion induced by the mixed salts (NaCl+CMA and NaCl+tr) fell between the pure chloride-based salts and the organic salts for MS and HS. In immersion conditions, the mass loss was greater for GS than for MS and HS in all salt solutions, 5–7 mg/cm^2 vs. 1.5–2 mg/cm^2. In both atmospheric and immersion conditions, there was little difference between the salts for GS. It is well documented that Zn corrodes more slowly than iron in a clean atmosphere [35,36]. This is due to the formation of a protective zinc carbonate patina ($ZnCO_3$) through wet-and-dry cycles that acts as a physical barrier to protect the base metal. However, this layer is not stable in salty environments [37,38], in which the formation of zinc hydroxide ($Zn(OH)_2$), simonkolleite ($Zn_5(OH)_8Cl_2{\cdot}H_2O$), and zinc oxide (ZnO) have been reported [15,39], and these corrosion products are much less stable than $ZnCO_3$.

The corrosivity of chloride-based salts towards the different investigated steel grades observed in this study is not surprising and has been well documented. It is caused by an increased uniform corrosion rate and destabilizes the protective films [40–44]. It is also well documented from previous comparative studies that the corrosion of low-alloy steel is inhibited by acetate ions in chloride-containing neutral solutions [45–49].

The corrosion of the GS was the exception among the steels, showing similar mass loss values for all eight salt types in both atmospheric and immersion conditions, while the other steels, as well as other alloys (stainless steel and aluminum alloy, presented in the Supporting Information in **sections S5 and S6**), clearly were more susceptible to the chloride-based salts. This trend is also clearly visible from the optical microscopy images (Fig. 1b and c) and microscopy images (**Figs. S5** and **S6** in **Section S7** in the Supporting Information).

Fig. 2 presents the released amounts of Zn or Fe from the steels after 168 h of immersion in the 0.5 M salt solutions. For GS, there was significant Zn release, while Fe concentrations remained negligible (below detection limits). This suggests that, within the studied exposure period, the Zn layer continued to provide protection to the underlying steel

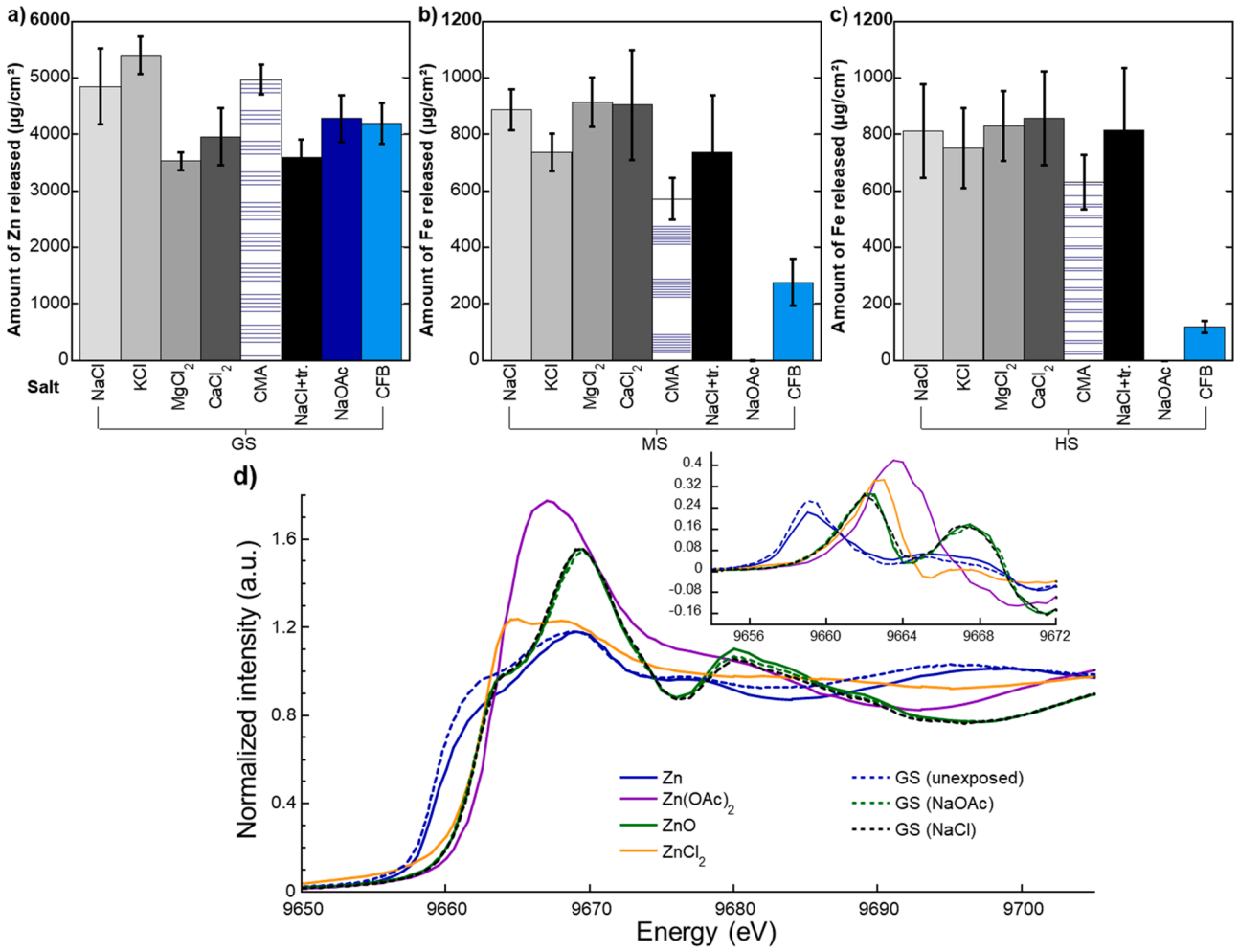

Fig. 2. Amounts of selected metals in solution (aqueous concentrations normalized to exposed surface area and solution volume) after 168 h immersion tests in 0.5 M salt solutions at room temperature: (a) Zn released from GS, (b) Fe released from MS, and (c) Fe released from HS. Average values and standard deviation (error bars) of triplicate samples are shown. Corresponding kinetic data (24 h and 168 h) and Cr, Mn, and Ni release data are shown in Section S8 in the Supporting Information. Note the different y-axis scales. CMA is an abbreviation for 95 wt. % NaCl + 5 wt. % CMA. Normalized Zn K-edge XANES of unexposed GS and GS after 168 h immersion tests in 0.5 M NaCl and 0.5 M NaOAc solution (d). The spectra of various reference materials (Zn metal, $ZnCl_2$, ZnO, and $Zn(OAc)_2$) are also shown. The inset in (d) shows the 1st derivative of the normalized XANES.

substrate, limiting Fe release. Similar to the mass loss after immersion or atmospheric conditions, the release of Zn from GS was similar in all eight salt solutions. The release of Fe from MS and HS was significantly smaller than that of Zn from GS. This is in line with the mass loss data presented in Fig. 1d. Similar to the mass loss data, Fe release from MS and HS is significantly higher in chloride-based salts than in the pure organic salts (NaOAc and CFB), Fig. 2a, which is consistent with previous studies [50].

Fig. 2b summarizes the comparison of the unexposed and exposed GS coupons to reference samples of Zn, ZnO, $ZnCl_2$, and $Zn(OAc)_2$ reference materials, measured by XANES. There was a high similarity between the Zn metal spectrum and that of unexposed GS. Likewise, both exposed GS coupons (to NaCl and NaOAc) showed a high resemblance with the reference sample ZnO, but neither $ZnCl_2$ nor $Zn(OAc)_2$. This was confirmed by linear combination fitting, revealing >95 % Zn for the unexposed GS and >95 % ZnO for the GS exposed to NaCl or NaOAc.

Section S3 and **Tables S2–S3** in the Supporting Information present the predicted equilibrium speciation and solubilities of Fe and Zn (by JESS modelling), as well as Cr, Ni, and Al for the alloys presented in **sections S5–S6** of the Supporting Information. The predicted solubility of Fe and Zn was primarily determined by pH and salt concentration. Acetate complexes were predicted in several cases, including for Zn, but not for Fe. To allow a fair comparison of Zn solubility values of NaCl and NaOAc solutions, JESS modelling was performed at the same pH (7.8) and concentration (0.5 M) for both the NaOAc and NaCl solutions. It would only slightly increase (to 5.6 mM in NaOAc compared with 3.7 mM in NaCl), so the predicted equilibrium speciation does not directly explain the experimental results, for which 32 mM Zn in NaOAc and 37 mM Zn in NaCl solution was detected for GS after one week of immersion.

In all, these solution analytical, corrosion product speciation, and speciation modelling results suggest that the insoluble corrosion product of GS in both NaCl and NaOAc solutions is ZnO, while the relatively high solubility of Zn into solution can be explained by a relatively higher solubility of chloride and acetate complexes with Zn compared to those with Fe.

3.2. Multi-analytical quantification of Zn corrosion of GS after immersion in NaCl and NaOAc

Based on the mass loss results, NaCl and NaOAc, as representatives for chloride-based and organic salts, were selected for further investigations of the salt- and material-specific interactions. Next, we quantified the Zn corrosion of GS after the 168 h-immersion to 0.5 M NaCl or 0.5 M NaOAc in relation to its initial Zn layer thickness. Cross-sectional analysis of GS before exposure and after exposure estimated

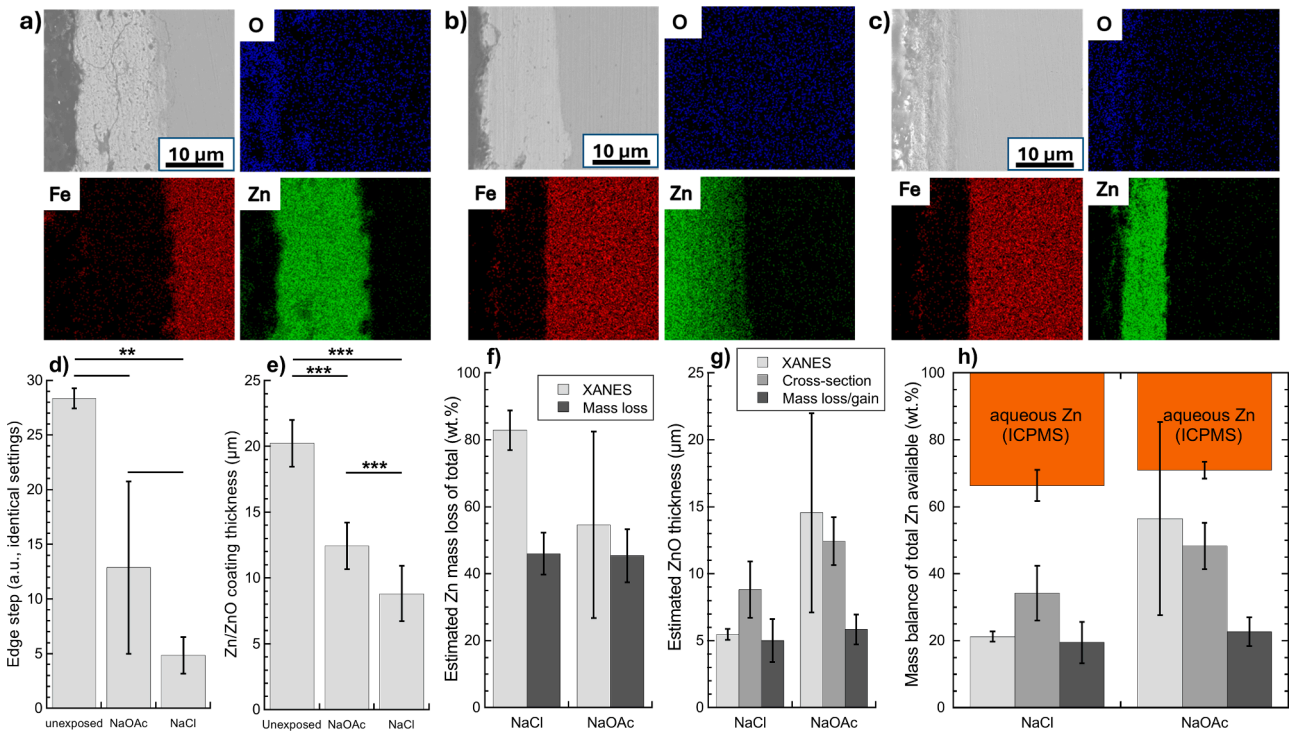

Fig. 3. Cross-section of GS in as-received and 168 h exposure to NaOAc and NaCl solutions. (a-c); representative cross-sectional SEM images and corresponding EDS elemental maps of GS: (a) as-received condition, (b) after exposure to NaOAc, and (c) after exposure to NaCl. Elemental distributions of Fe, Zn, and O are presented to show the coating structure, Zn layer thickness, and the spatial distribution of corrosion products across the coating/substrate interface. (d) Comparison of the edge step (directly proportional to the Zn content) of three different locations (mean and the standard deviations shown as the error bars) of unexposed GS and GS after 168 h immersion tests in 0.5 M NaCl and 0.5 M NaOAc solution. (e) Cross-sectional analysis of GS showing the average remaining Zn layer thickness in the as-received condition and after 168 h exposure to NaCl and NaOAc solutions. Thickness values were obtained from four independent locations per sample, with at least five measurements per location ($n = 20$). Error bars represent the standard deviation from multiple measurements obtained across different regions of each sample. (f) Comparison of Zn mass loss after 168 h exposure of GS to 0.5 M NaCl or 0.5 M NaOAc across two different techniques (XANES and cross-section analysis) as wt. % of total available Zn based on cross-sectional thickness analysis of the unexposed GS. (g) Estimation of ZnO thickness after 168 h exposure of GS to 0.5 M NaCl or 0.5 M NaOAc from three independent techniques (XANES, cross-section, and mass measurements), assuming ZnO as the only remaining composition (as per XANES in Fig. 2d) and its density to be 5.61 g/cm^3. (h) Total mass balance across four techniques, estimating the amount of Zn (as wt. % of total available based on cross-section analysis of the unexposed GS), converting into solid ZnO (estimated for XANES, cross-section analysis, and mass measurements, same legend as in (g)) and into soluble aqueous phases (as measured by ICPMS, orange, from top). ** $p < 0.01$; *** < 0.0001.

the initial zinc layer thickness and final ZnO thickness. Representative cross-sectional SEM images and corresponding EDX elemental maps are presented in Fig. 3a–c. In the as-received condition (Fig. 3a), a continuous and well-defined Zn layer was present on the steel substrate. Following exposure to both salt solutions (0.5 M NaOAc or NaCl), the Zn layer thickness decreased and an oxygen-rich outer region developed, consistent with the formation of corrosion products of ZnO (Fig. 2d). The elemental distributions of the EDX mappings indicate that the Zn signal decreased toward the outer surface, while Fe remained largely confined to the substrate, suggesting that, despite the significant Zn dissolution, the coating still provided partial protection to the underlying steel within the exposure period.

Fig. 3d summarizes quantitative insights from the XANES measurements. For this hard X-ray technique (penetrating the entire Zn layer in all cases) and by using identical optical settings, it was possible to compare the Zn content of unexposed GS and that of GS exposed to the NaOAc and NaCl solutions. Three different locations were measured on each of these coupons. The variability after NaOAc exposure was highest, indicating differences in Zn layer thickness across the three spots. The relative variability of the Zn content/thickness increased from the as-received control (3.2 %) to the NaCl-exposed (34.5 %) and the NaOAc-exposed (61.4 %) coupons, indicating non-uniform mass loss processes. Twenty cross-sectional lengths of the Zn coating (unexposed) or the ZnO corrosion product (after 168 h immersion exposure to either 0.5 M NaCl or 0.5 M NaOAc) were averaged and are shown in Fig. 3e, also revealing significant thickness reductions after exposure, with slightly more thickness reduction for NaCl than NaOAc, similar to the XANES estimations in Fig. 3d. Fig. 3e–d were further converted into Zn mass loss expressed as wt. % of total available Zn, based on the cross-sectional thickness analysis of the unexposed GS, revealing >40 wt. % Zn lost, Fig. 3f. Fig. 3g compares estimations of the ZnO thickness across three techniques, assuming that all Zn in the solid corrosion product is in the form of ZnO (as per Fig. 2d), showing about 5–15 µm remaining out of the initial 20 µm of metallic Zn. These results were further converted into wt. % of available total Zn and compared to the Zn in the solution phase, measured by ICPMS, in Fig. 3h. Theoretically, this should add up to 100 wt. %. The closest estimate was achieved with XANES and the cross-sectional analysis of the solid corrosion product and ICPMS. XANES may have underestimated the solid corrosion product in the case of NaCl exposure, and the measured masses (initial mass, mass after exposure, and mass after the pickling procedure) may have underestimated the solid corrosion product mass for both salt solutions, which can be related to underpickling. Likewise, the ICPMS-estimated aqueous Zn can be underestimated due to analyte loss, as the concentrations were higher than the predicted solubility (Section 3.1).

In all, all four techniques show very clearly that a significant amount of the coated Zn is corroded after one week of immersion in 0.5 M NaCl or 0.5 M NaOAc, of which slightly less than half is solubilized and the remaining part is a solid corrosion product. It is interesting to note that the even higher mass loss observed for the field tests (Fig. 1) for GS exposed by a spray bottle once a week must hence include mass from the underlying steel, possibly by exposure of the edges or non-uniform

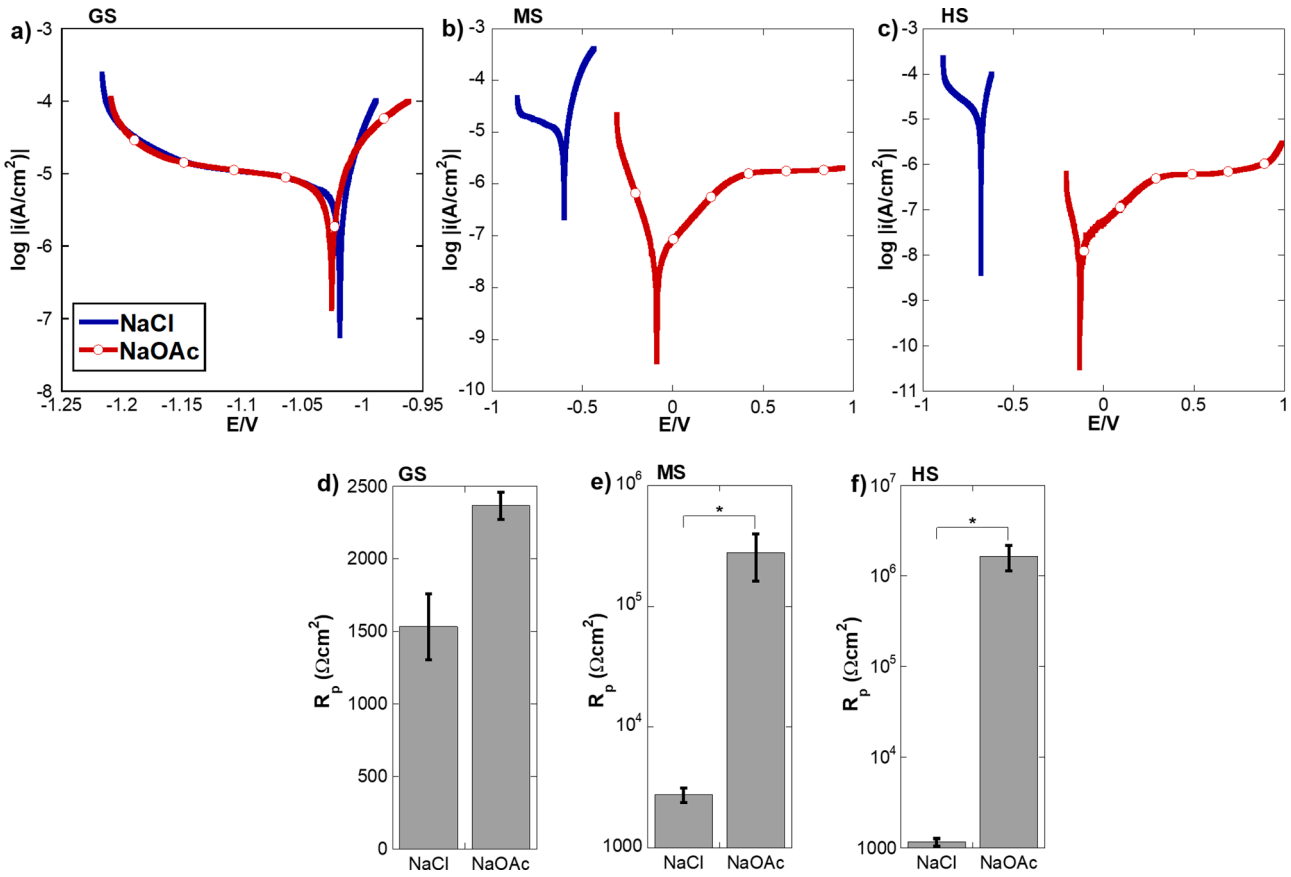

Fig. 4. Comparative electrochemical behavior of GS, MS, and HS in 0.1 M NaCl and NaOAc solutions at room temperature using potentiodynamic polarization (PDP) and linear polarization resistance (LPR) techniques: (a), (b), and (c) are PDP curve of GS, MS and HS, respectively. (d), (e), and (f) show the R_p of GS, MS, and HS respectively. The R_p values show the average and standard deviation (error bars) of triplicate samples, while the PDP curves are representative curves. The asterisk (*) indicates a statistically significant difference ($p < 0.05$) between two sets of triplicate samples. The y-axes of e and f are on a logarithmic scale. The voltage is against a Ag/AgCl sat. KCl reference electrode.

Table 3
A summary of electrochemical parameters extracted from the PDP curves, showing average and standard deviation of triplicate samples of GS, MS, and HS, in 0.1 M NaCl, NaOAc, or $Zn(OAc)_2$ solutions at room temperature. The corrosion potential (E_{corr}), Tafel parameters (β_a, β_c), and corrosion current density (i_{corr}) are shown.

Metals	Salts	E_{corr} (V)	Cathodic β_c (mV/dec)	Anodic β_a (mV/dec)	Corrosion current density i_{corr} (A/cm^2)
GS	NaCl	−1.09 ± 0.02	49 ± 9	28 ± 4	(1.1 ± 0.7) × 10^{-6}
	NaOAc	−1.03 ± 0.01	69 ± 23	32 ± 14	(4.2 ± 1.6) × 10^{-6}
	$Zn(OAc)_2$	−1.02 ± 0.004	49 ± 16	38 ± 5	(14 ± 2.5) × 10^{-6}
MS	NaCl	−0.65 ± 0.06	247 ± 67	63 ± 15	(4.3 ± 2.8) × 10^{-6}
	NaOAc	−0.17 ± 0.15	99 ± 9	212 ± 92	(0.26 ± 0.4) × 10^{-6}
	$Zn(OAc)_2$	−0.35 ± 0.29	54 ± 19	102 ± 18	(2.3 ± 3.6) × 10^{-6}
HS	NaCl	−0.57 ± 0.19	90 ± 13	27 ± 14	(4.8 ± 3.0) × 10^{-6}
	NaOAc	−0.12 ± 0.04	69 ± 36	294 ± 39	(0.05 ± 0.03) × 10^{-6}
	$Zn(OAc)_2^a$	−0.62 ± 0.02	32 ± 2	55 ± 22	(4.9 ± 2.6) × 10^{-6}

Corrosion potentials (E_{corr}) are reported in V *vs.* $Ag/AgCl_{(sat.)}$. Corrosion current densities (i_{corr}) are expressed in A/cm^2. [a] – only two replicates.

corrosion. Nevertheless, it is very clear from all results presented so far that all salt solutions are very corrosive to GS, while only chloride-containing salts are corrosive to MS and HS (and at a lower rate).

3.3. Electrochemical and solution insights

Fig. 4a–c present representative potentiodynamic polarization (PDP) curves of GS, MS, and HS in 0.1 M NaCl or NaOAc. Summarized results from such plots are shown in Table 3. GS showed a similar corrosion current in both NaCl and NaOAc salt solutions, in contrast to MS and HS (Table 3), which showed higher (>10-fold) corrosion currents in NaCl than NaOAc. This was confirmed by LPR measurements (Fig. 4d–f), which showed statistically significant ($p < 0.05$, two orders of magnitude) higher polarization resistance (R_p) values for MS and HS in NaOAc than in NaCl solution. Both results show that the chloride-based salt is more corrosive to MS and HS than the organic salt. Similar trends were found for other chloride-based salts (**Section S9** in the Supporting Information).

In contrast to the commonly reported lower corrosivity of acetate-based salts for steels [51,52], the present study shows that GS undergoes significant degradation in both chloride-based and acetate-based salts. While NaCl exposure resulted in slightly greater overall Zn mass loss (Figs. 1–3), NaOAc exposure produced comparable GS degradation, accompanied by significantly higher variability in the remaining Zn layer. While this has rarely been studied in the literature, it does align with previous studies on Zn-Al-Mg hot-dip galvanized steel, finding a porous oxide in the presence of NaOAc [53].

If the high corrosion susceptibility of GS to NaOAc were determined

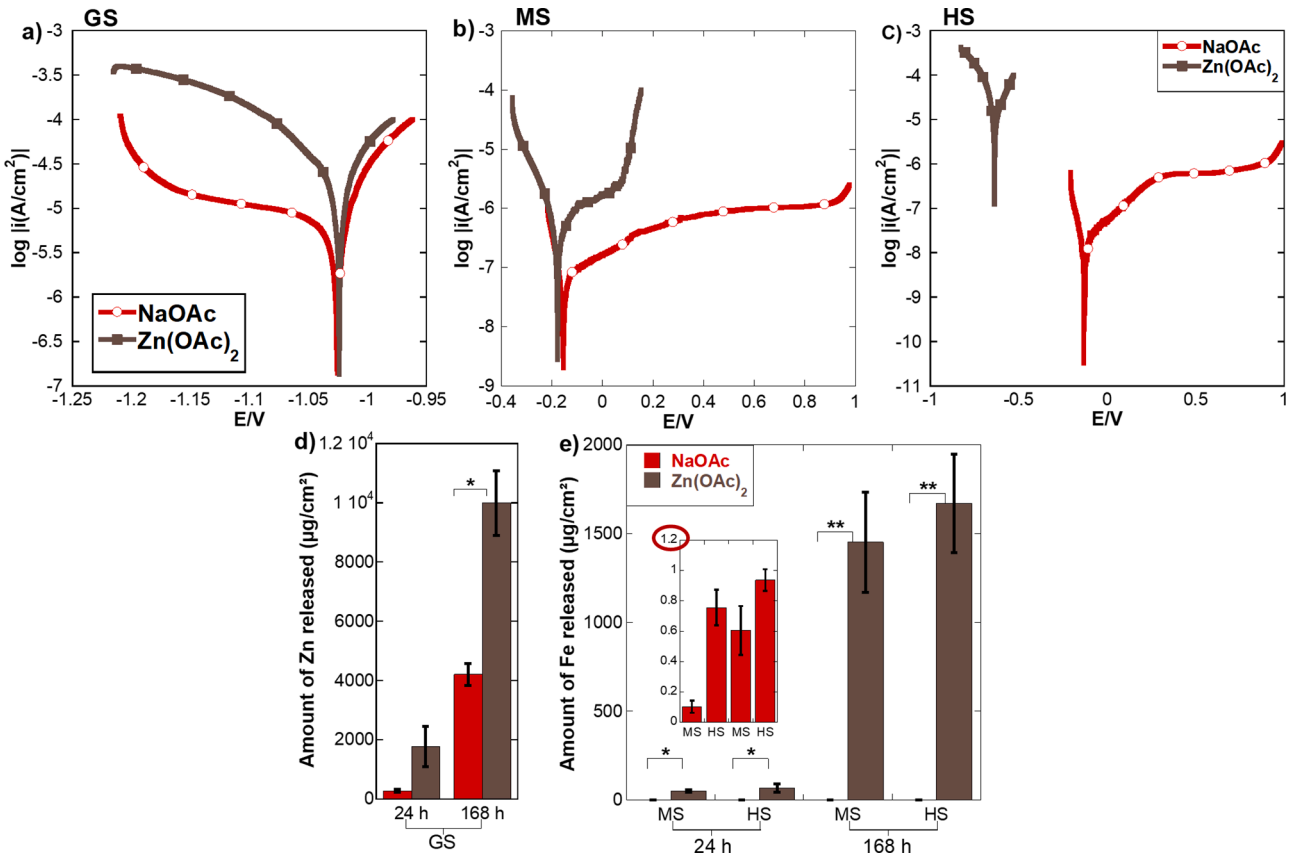

Fig. 5. Comparative electrochemical behaviour of GS (a), MS (b), and HS (c) in 0.1 M NaOAc and 0.1 M $Zn(OAc)_2$ solutions at room temperature using potentiodynamic polarization (PDP). The PDP curves are representative curves, and the voltage is against an Ag/AgCl(sat.) reference electrode. Extracted parameters are shown in Table 3. Amounts of zinc (d) released from GS and iron (e) released from MS and HS into solution (aqueous concentrations normalized to exposed surface area and solution volume) after 24 and 168 h immersion tests in 0.5 M NaOAc and 0.5 M $Zn(OAc)_2$ solutions at room temperature. Average values and standard deviation (error bars) of triplicate samples are shown. Note the different y-axis scales. The asterisks indicate a statistically significant difference (* $p < 0.05$; ** $p < 0.01$) between two sets of triplicate samples.

by Zn alone, we would expect a mass loss corresponding to the Zn layer thickness, followed by a mass loss corresponding to that of steel in NaOAc. However, from the calculations in Fig. 3 and the mass loss determined for GS from the field tests exposed to NaOAc (Fig. 1), it is clear that GS is corroding more than the total mass of its Zn layer would predict. Hence, the underlying steel corroded more when exposed to NaOAc than MS and HS (without Zn) did in NaOAc. Similarly, we found in preliminary experiments that the GS corrosion and Fe release from GS were greater than those of MS and HS, when the zinc layer was not entirely covering the surface (Supporting Information **Fig. S10**). This suggests that the underlying process involves at least three components: the steel, the Zn layer or Zn ions, and acetate ions.

To further decipher the mechanism of increased corrosion of GS within acetate or other organic ligand environments, we also conducted electrochemical and immersion tests in 0.1 M $Zn(OAc)_2$ solutions and compared those to the results in 0.1 M NaOAc solution. If it is true that both the presence of zinc and acetate are required for the increased corrosion rate of steels, then iron-containing alloys without zinc coatings should have a higher corrosion rate in $Zn(OAc)_2$ than in NaOAc solutions.

Fig. 5a–c present representative PDP curves of GS, MS, and HS immersed in NaOAc and $Zn(OAc)_2$ solutions (corresponding extracted parameters in Table 3) For GS, the difference in corrosion current density between the NaCl and NaOAc solutions is not statistically significant, but it is significantly ($p < 0.01$) higher in the $Zn(OAc)_2$ solution compared to both NaCl and NaOAc solutions. For both MS and HS, the differences in the current densities are not statistically significant due to some variability, but the absolute difference shows the same trend for both steels: the corrosion current density is 10-fold and 100-fold smaller in NaOAc solution compared to both NaCl and $Zn(OAc)_2$ solutions for MS and HS, respectively. Further, Fig. 5d–e show the corresponding increase in metal release of Zn from GS and of Fe from MS and HS after 24 and 168 h of immersion at room temperature, induced by the presence of 0.5 M $Zn(OAc)_2$ as compared to 0.5 M NaOAc solution. The 2400–12,000-fold increase of Fe release from MS and HS in $Zn(OAc)_2$ compared with NaOAc solution is highly statistically significant.

In all, these results confirm our suspicion that steel corrosion is accelerated in the presence of both zinc and acetate.

3.7. *Further discussion*

This study clearly demonstrated that the three-component system (steel, zinc, and acetate) can induce corrosion in steels exposed to zinc and acetate. This corrosion goes beyond a two-component process: the corrosion rate is greater than what would be expected from acetate-induced dissolution of zinc, followed by a system of steel exposed to acetate. A closer look at the anodic and cathodic branches in the PDP curves of GS *versus* MS and HS in NaOAc environments (Figs. 4 and 5, Table 3) reveals that the cathodic slope was relatively similar in NaOAc for all three steels, but there was a much higher anodic slope/current (lower β_a) in the presence of Zn and acetate (either in $Zn(OAc)_2$ solution or for GS in NaOAc). This suggests that the increased dissolution of Zn from GS is not caused by a catalytic effect, which would increase the cathodic reactions, but that the anodic dissolution of steel is strongly increased in the presence of acetate and either Zn metal or ions. This study cannot determine the underlying chemical reason for the

increased Fe dissolution from steels in the presence of Zn and acetate, but in general, it could be caused through two pathways: (*i*) difference in passivity, for example through different kinetics of the formation, or speciation of Fe corrosion products influenced by the Zn, and (*ii*) faster dissolution rate of Fe-containing corrosion products influenced by Zn. A Zn ion-induced increased solubility (decreased passivity) of iron oxides in acetate environments is, however, unlikely. Although there have been few studies on the effect of zinc ions on the dissolution of iron oxides, the few studies that do exist point towards a *lower* dissolution rate of iron oxides and hydroxides if zinc ions are adsorbed or incorporated [54,55]. It is, however, known that Zn ions easily adsorb on iron oxides [56], so future studies should investigate whether the observed vastly increased Fe dissolution of steels in $Zn(OAc)_2$ *vs.* NaOAc solutions in this study and the drastically increased anodic branch in the PDP curves indeed is caused by an accelerated iron oxide dissolution process. Although we consider it unlikely that zinc ions would be reduced by the steel under the experimental conditions, further studies should also consider galvanic effects.

While outside of the scope of the present study, we highly encourage future studies of the corrosion behavior of other infrastructure alloys in organic de-icers. Our preliminary results showed that $Zn(OAc)_2$ might also be detrimental to aluminum alloys (Supporting Information, **Section S6**), which might have implications for some systems, such as galvalume-protected steels. Our findings challenge the prevailing assumption that organic salts, particularly acetates, are universally less corrosive than chlorides when applied as de-icers. Infrastructure containing galvanized components may therefore be at significant risk if acetate-based salts are adopted as "green" alternatives. The practical implication of this work is that caution is needed when planning for alternative road de-icing salts around outdoor infrastructure containing galvanized steel. This contradicts initial expectations that acetate-based salts would cause less corrosion than chloride-based salts for all structural alloys [57].

4. Conclusions

The objective of this study was to investigate the corrosion susceptibility of galvanized, mild, and high-strength steel when exposed to inorganic and organic de-icing agents. Galvanized steel corroded almost equally by various types of salts, both inorganic and organic, in both atmospheric and immersion exposure conditions and in electrochemical tests. While chloride-containing solutions induced substantial and relatively uniform corrosion of galvanized steel, acetate-containing environments also led to significant degradation of the Zn and cannot be considered benign. Sodium acetate resulted in more corrosion of galvanized steel than was explainable by acetate-induced zinc dissolution alone. In fact, the corrosion of galvanized steel was more than the sum of zinc dissolution and acetate-induced corrosion of steel. This inspired us to look into a three-component system: steel (Fe), zinc metal/ions, and acetate ions. Electrochemical and solution-analytical measurements revealed that acetate-containing solutions, in the presence of dissolved Zn species, promote conditions that facilitate Fe dissolution. This seemed to be a process involving the destabilization of the iron (hydr)oxide, rather than an effect on the cathodic reactions. After immersion in sodium chloride or acetate solutions, the prevailing corrosion product on galvanized steel was ZnO, and thermodynamic equilibrium speciation modelling suggested that complexes of Zn chlorides and acetates were aqueous. A mass balance calculation via mass loss/gain, XANES, cross-section, and ICPMS methods, revealed a large fraction (>40 wt. %) of the 20 μm-thick galvanized zinc layer to be in solution after one week of immersion in 0.5 M sodium chloride or sodium acetate. Likewise, no metallic zinc (only some ZnO) was remaining after this one-week immersion or the 10-week atmospheric field exposure (sprayed once a week with 0.1 g/L salt brine). This shows the highly corrosive nature of chloride-based and alternative de-icer road salts to galvanized steel. Organic alternative road salts might be as corrosive as traditional chloride-based salts to galvanized steel, which needs to be considered.

Data availability

Coding, reactions, conditions, and results of the chemical speciation modelling, and all raw data to the figures shown in this paper are available on https://osf.io/xydba/overview?view_only=7b83a40b426b4e6d83c4f54116a7812f.

Funding

This work was supported by the Natural Sciences and Engineering Research Council of Canada [grant numbers ALLRP 571358–2021, CREATE 565232–2022, DGDND-2021–03997, RGPIN-2021–03997]; MITACS [grant number IT28967]; Cypher Environmental Ltd. [ALLRP 571358–2021]; the Canada Research Chairs Program [grant number CRC-2019–00425]; the Ontario Ministry of Colleges and Universities [Ontario Research Fund – Small Infrastructure Fund, 42507], the Canada Foundation for Innovation [John R. Evans Leaders Fund, 42507], the Infrastructure Operating Fund [0000056276]; startup funds at Western University, Canada (Dept. Chemistry, 2020); Western Sustainable Impact Fund [2024 Robert Addai]; and the Wolfe-Western Fellowship [grant number 2020].

CRediT authorship contribution statement

R. Addai: Conceptualization, Methodology, Validation, Formal analysis, Investigation, Writing – original draft, Visualization, Funding acquisition. **S. Ramamurthy:** Methodology, Validation, Formal analysis, Investigation, Writing – review & editing, Visualization. **D. Zagidulin:** Methodology, Validation, Formal analysis, Investigation, Writing – review & editing, Visualization. **Z. Wang:** Investigation, Methodology, Formal analysis, Writing – review & editing. **C. Power:** Writing – review & editing, Funding acquisition. **J.M.C. Mol:** Conceptualization, Validation, Supervision, Writing – review & editing. **Y.S. Hedberg:** Conceptualization, Methodology, Validation, Formal analysis, Investigation, Resources, Writing – review & editing, Visualization, Supervision, Project administration, Funding acquisition.

Declaration of competing interest

The authors declare the following financial interests/personal relationships which may be considered as potential competing interests:

Yolanda Hedberg reports financial support was provided by Natural Sciences and Engineering Research Council of Canada. Chris Power reports financial support was provided by Natural Sciences and Engineering Research Council of Canada. Yolanda Hedberg reports financial support was provided by Mitacs Inc. Chris Power reports financial support was provided by Mitacs Inc. Yolanda Hedberg reports financial support was provided by Canada Research Chairs Program. Yolanda Hedberg reports financial support was provided by Ontario Ministry of Colleges and Universities. Yolanda Hedberg reports financial support was provided by Fondation canadienne pour l'innovation. Yolanda Hedberg reports financial support was provided by Infrastructure Operating Fund. Yolanda Hedberg reports financial support was provided by Cypher Environmental Ltd. Chris Power reports financial support was provided by Cypher Environmental Ltd. If there are other authors, they declare that they have no known competing financial interests or personal relationships that could have appeared to influence the work reported in this paper.

Acknowledgments

We thank Dr. Jonas Hedberg for help with the inductively coupled plasma mass spectrometry, Dr. Marshall Yang for initial training in

electrochemical experimental testing and plotting of electrochemical data (all of these at Western University), and Agnieszka Kooijman for initial training in electrochemical experimental testing and data analysis (Delft University of Technology). We thank Cypher Environmental Ltd., in particular Dr. Teaghan Wellman and Trent Adams, for valuable discussions and the provision of some of the de-icing salts tested in this study. We thank SSAB AB (Borlänge, Sweden), Outokumpu Nirosta GmbH (Krefeld, Germany), and Delft University Technology, the Netherlands, for providing some of the alloys and valuable discussions, respectively. We also thank Dr. Dirk Wiemer (Outokumpu), Ulf Bexell (SSAB), and Dr. Rachel Pettersson (Jernkontoret) for valuable discussions about the steels. We also thank Diamond Light Source (United Kingdom) for the beam time allocation (SP41814) at beamline I18 and Dr. Susan Nehzati for assistance during the experiments. The staff at Surface Science Western is also acknowledged for assistance in surface analysis.

Supplementary materials

Supplementary material associated with this article can be found, in the online version, at doi:10.1016/j.electacta.2026.149030.

References

[1] H.Ullah Sajid, D.L. Naik, R. Kiran, Improving the ice-melting capacity of traditional deicers, Constr. Build. Mater. 271 (2021) 121527.
[2] Y. Tian, W. Guo, J. Cao, B. Wang, P. Wang, P. Zhang, T. Zhao, Influence of NaCl on the ice formation process in ordinary and air-entrained mortar based on LF-NMR, J. Mater. Res. Technol. 24 (2023) 1322–1334.
[3] T. Liang, Y. Lai, D. Hou, Q. Yang, Y. Yang, R. Bai, J. Zhang, J. Jiang, Freezing mechanism of NaCl solution ultra-confined on surface of calcium-silicate-hydrate: a molecular dynamics study, Cem. Concr. Res. 154 (2022) 106722.
[4] F. Autelitano, M. Rinaldi, F. Giuliani, Winter highway maintenance strategies: are all the sodium chloride salts the same? Constr. Build. Mater. 226 (2019) 945–952.
[5] S. Szklarek, A. Górecka, A. Wojtal-Frankiewicz, The effects of road salt on freshwater ecosystems and solutions for mitigating chloride pollution - a review, Sci. Total Environ. 805 (2022) 150289.
[6] S. Szklarek, A. Górecka, B. Salabert, A. Wojtal-Frankiewicz, Acute toxicity of seven de-icing salts on four zooplankton species– is there an “eco-friendly” alternative? Ecohydrol. Hydrobiol. 22 (2022) 589–597.
[7] R.R. Horner, M.V. Brenner, Environmental evaluation of calcium magnesium acetate for highway deicing applications, Resour. Conserv. Recycl. 7 (1992) 213–237.
[8] Z. Lu, C. Liu, K. Xu, Q. Wang, Initial corrosion behavior and novel chloride threshold determination methods for carbon steel in simulated concrete pore solution based on 1D pit test and CPP test, Electrochim. Acta 540 (2025) 147213.
[9] S. Sharifi-Asl, F. Mao, P. Lu, B. Kursten, D.D. Macdonald, Exploration of the effect of chloride ion concentration and temperature on pitting corrosion of carbon steel in saturated Ca(OH)2 solution, Corros. Sci. 98 (2015) 708–715.
[10] N. Ebrahimi, M. Roshanfar, M. Momeni, O.J. Naboka, Corrosion performance of atmospheric corrosion resistant steel bridges in the current climate: a performance review, Materials 18 (2025) 3510.
[11] X. Shi, L. Fay, Z. Yang, T.A. Nguyen, Y.J. Liu, Corrosion of deicers to metals in transportation infrastructure: introduction and recent developments, Corros. Rev. 27 (2009) 23–52.
[12] M.I. Hussain, S. Nawaz, M.M. Sajid, A. Nawaz, A. Irum, Y. Javed, C. Ge, G. Yasin, Chapter 5 - corrosion resistance of nanostructured metals and alloys, corrosion protection at the nanoscale, Elsevier (2020) 63–87, https://doi.org/10.1016/B978-0-12-819359-4.00005-2.
[13] J.-E. Svensson, L.-G.J. Johansson, A laboratory study of the initial stages of the atmospheric corrosion of zinc in the presence of NaCl; influence SO2 NO2, Corros. Sci. 34 (1993) 721–740.
[14] M. Abankar, M. De Maddis, V. Razza, P.J. Russo Spena, Resistance element welding (REW) of steels with non-ferrous materials: potentials, challenges, and properties, Metals 14 (2024) 1448.
[15] Y. Meng, L. Liu, D. Zhang, C. Dong, Y. Yan, A.A. Volinsky, L.-N. Wang, Initial formation of corrosion products on pure zinc in saline solution, Bioact. Mater. 4 (2019) 87–96.
[16] A. Kaleva, T. Tassaing, V. Saarimaa, G. Le Bourdon, P. Väisänen, A. Markkula, E. Levänen, Formation of corrosion products on zinc in wet supercritical and subcritical CO2: in-situ spectroscopic study, Corros. Sci. 174 (2020) 108850.
[17] S. Zhang, X. He, T. Shang, G. Jiang, W. Liu, H. Teng, T. Chen, X. Cheng, C. Liu, The initial corrosion mechanism of hot-dipping Zn–Al–Mg alloy coating in chloride-containing solution, J. Mater. Sci. 59 (2024) 20780–20795.
[18] E. Diler, B. Rouvellou, S. Rioual, B. Lescop, G. Nguyen Vien, D. Thierry, Characterization of corrosion products of Zn and Zn–Mg–Al coated steel in a marine atmosphere, Corros. Sci. 87 (2014) 111–117.
[19] G. Kilincceker, H. Galip, Electrochemical behaviour of zinc in chloride and acetate solutions, Prot. Met. Phys. Chem. Surf. 45 (2009) 232–240.
[20] S. Valet, T. Bohlmann, A. Burkert, G. Ebell, Zinc acetate containing gel pads for electrochemical measurements of Zn samples, J. Electroanal. Chem. 948 (2023) 117814.
[21] S.J. Borg, W. Liu, An XAS study of zinc speciation in aqueous acetate solutions at 25–200 °C, Nuclear Instruments and Methods in Physics Research Section A: accelerators, spectrometers, Detect. Assoc. Equip. 619 (2010) 276–279.
[22] M. Ahangar, M. Izadi, T. Shahrabi, I. Mohammadi, The synergistic effect of zinc acetate on the protective behavior of sodium lignosulfonate for corrosion prevention of mild steel in 3.5 wt% NaCl electrolyte: surface and electrochemical studies, J. Mol. Liq. 314 (2020) 113617.
[23] V. Padilla, P. Ghods, A. Alfantazi, Effect of de-icing salts on the corrosion performance of galvanized steel in sulphate contaminated soil, Constr. Build. Mater. 40 (2013) 908–918.
[24] A.K. Perka, M. John, U.B. Kuruveri, P.L. Menezes, Advanced high-strength steels for automotive applications: Arc and laser welding process, properties, and challenges, Metals 12 (2022) 1051.
[25] D. de la Fuente, I. Díaz, J. Simancas, B. Chico, M.J.C.S. Morcillo, Long-term atmospheric corrosion of mild steel, Corros. Sci. 53 (2011) 604–617.
[26] R. Vera, B. Valverde, E. Olave, R. Sánchez, A. Díaz-Gómez, L. Muñoz, P. Rojas, Atmospheric corrosion and impact toughness of steels: case study in steels with and without galvanizing, exposed for 3 years in Rapa Nui Island, Heliyon. 9 (2023) e17811.
[27] G. Ke, J. Zhang, B. Tian, Evaluation and selection of de-icing salt based on multi-factor, Mater. (Basel) 12 (2019) 912.
[28] M. Atapour, X. Wang, M. Persson, I. Odnevall Wallinder, Y.S. Hedberg, Corrosion of binder jetting additively manufactured 316L stainless steel of different surface finish, J. Electrochem. Soc. 167 (2020) 131503.
[29] Y.S. Hedberg, S. Goidanich, G. Herting, I.Odnevall Wallinder, Surface–rain interactions: differences in copper runoff for copper sheet of different inclination, orientation, and atmospheric exposure conditions, Environ. Pollut. 196 (2015) 363–370.
[30] ASTM International, Metals, Standard practice For preparing, cleaning, and Evaluating Corrosion Test Specimens, ASTM International, 2017, pp. G1–03.
[31] B. Ravel, M. Newville, ARTEMIS ATHENA, HEPHAESTUS: data analysis for X-ray absorption spectroscopy using IFEFFIT, Synchrotron Radiat. 12 (2005) 537–541.
[32] P. May, JESS at thirty: strengths, weaknesses and future needs in the modelling of chemical speciation, Appl. Geochem. 55 (2014) 3–16.
[33] A. vander Zee, L. Laundry-Mottiar, S. Nikpour, S. Matin, J. Henderson, U. Eduok, J. Hedberg, D. Zagidulin, M. Biesinger, J. Noël, Y. Hedberg, Effect of amino acids on the corrosion and metal release from copper and stainless steel, J. Electrochem. Soc. 170 (2023) 021501.
[34] P.M. May, D. Rowland, E. Königsberger, G. Hefter, a JESS, Joint Expert Speciation System–IV: a large database of aqueous solution physicochemical properties with an automatic means of achieving thermodynamic consistency, Talanta 81 (2010) 142–148.
[35] ISO 9223:2012, Corrosion of metals and alloys - Corrosivity of atmospheres - classification, determination and estimation, International Standard Organization, 2012.
[36] L. Paterlini, A. Brenna, F. Ceriani, M. Gamba, M. Ormellese, F.M. Bolzoni, Atmospheric corrosion of different steel types in urban and marine exposure, Mater. (Basel) 17 (2024) 6211.
[37] F. Zhu, D. Persson, D. Thierry, C. Taxén, Formation of corrosion products on open and confined zinc surfaces exposed to periodic wet/dry conditions, Corrosion 56 (2000) 1256–1265.
[38] V. Saarimaa, A. Kaleva, A. Ismailov, T. Laihinen, M. Virtanen, E. Levänen, P. Väisänen, Corrosion product formation on zinc-coated steel in wet supercritical carbon dioxide, Arab. J. Chem. 15 (2021) 103636.
[39] J. Duchoslav, R. Steinberger, M. Arndt, D. Stifter, XPS study of zinc hydroxide as a potential corrosion product of zinc: rapid X-ray induced conversion into zinc oxide, Corros. Sci. 82 (2014) 356–361.
[40] E.F. Daniel, C. Wang, C. Li, J. Dong, I.I. Udoh, D. Zhang, W. Zhong, S. Zhong, Evolution of corrosion degradation in galvanised steel bolts exposed to a tropical marine environment, J. Mater. Res. Technol. 27 (2023) 5177–5190.
[41] M.S.D.A.B. da Fonsêca, G.R. Meira, Accelerated chloride-induced corrosion of hot-dipped galvanized reinforcements and its influence on bond strength to concrete, Constr. Build. Mater. 426 (2024) 136123.
[42] I.M. Ismail, O.E. Abdel-Salam, T.S. Ahmed, A. Soliman, M.F. Al-Ebrahim, I.A.J.P.E. A. Khattab, Investigation of the anodic dissolution of zinc in sodium chloride electrolyte–a green process, Port. Electrochim. Acta 31 (2013) 207–219.
[43] P. Li, M.J.C.C. Du, Effect of chloride ion content on pitting corrosion of dispersion-strengthened-high-strength steel, Corros. Commun. 7 (2022) 23–34.
[44] S. Ahmed, Y. Hou, K. Lepkova, T.J.C. Pojtanabuntoeng, M. Degradation, Investigation of the effect chloride ions on carbon steel in closed environments at different temperatures, Corros. Mater. Degrad. 4 (2023) 364–381.
[45] M.-O. Danyliak, I. Zin, S.A. Korniy, Corrosion inhibition of low-alloy carbon steel by gum arabic and zinc acetate in neutral chloride-containing environment, J. Ind. Eng. Chem. 129 (2024) 267–277.
[46] K. Takahashi, J.A. Bardwell, B. MacDougall, M.J. Graham, Mechanism of anodic dissolution and passivation of iron—I. behavior in neutral acetate buffer solutions, Electrochim. Acta 37 (1992) 477–487.
[47] X.-P. Guo, Z. Chen, D. Liu, K. Bando, Y. Tomoe, The effect of acetic acid and acetate on CO2 corrosion of carbon steel, CORROSION 2005, Assoc. Mater. Prot. Perform. (2005) C2005–05306.
[48] H.-S. Ryu, D.-M. Kim, S.-H. Shin, W.-J. Park, S.-J. Kwon, Steel-corrosion characteristics of an environmental inhibitor using limestone sludge and acetic acid, Int. J. Concr. Struct. Mater. 12 (2018) 13.

[49] F.M. Galleguillos Madrid, A. Soliz, L. Cáceres, M. Bergendahl, S. Leiva-Guajardo, C. Portillo, D. Olivares, N. Toro, V. Jimenez-Arevalo, M. Páez, Green corrosion inhibitors for metal and alloys protection in contact with aqueous saline, Mater. (Basel) 17 (2024) 3996.
[50] D.S. Azambuja, L.R. Holzle, I.L. Muller, C.M.S. Piatnicki, Electrochemical behaviour of iron in neutral solutions of acetate and benzoate anions, Corros. Sci. 41 (1999) 2083–2097.
[51] K.J. Kennelley, C.E. Locke Jr., Electrochemical behavior of steel in calcium magnesium acetate, Corrosion 46 (1990) 888–895.
[52] J.S. Gulliver, C.L. Chun, P.T. Weiss, A.J. Erickson, W. Herb, J. Henneck, K. Cassidy, Environmental Impacts of Potassium Acetate As a Road Salt Alternative (University of Minnesota evaluation), Minnesota Department of Transportation, 2022. https://hdl.handle.net/11299/242010.
[53] T. Keppert, G. Luckeneder, K.H. Stellnberger, G. Mori, H.J.M. Antrekowitsch, Corrosion, the effect of sulphate, phosphate, nitrate and acetate on the corrosion behaviour of Zn–Al–Mg hot-dip galvanised steel, Mater. Corros. 65 (2014) 560–568.
[54] M.V. Biber, M. dos Santos Afonso, W. Stumm, The coordination chemistry of weathering: IV. inhibition of the dissolution of oxide minerals, Geochim. Cosmochim. Acta 58 (1994) 1999–2010.
[55] J.D. Hem, Reactions of metal ions at surfaces of hydrous iron oxide, Geochim. Cosmochim. Acta 41 (1977) 527–538.
[56] V. Uygur, D.L. Rimmer, Reactions of zinc with iron-oxide coated calcite surfaces at alkaline pH, Eur. J. Soil. Sci. 51 (2000) 511–516.
[57] L. Terry, K. Conaway, J. Rebar, A. Graettinger, Alternative deicers for winter road maintenance—a review, Water Air Soil Pollut. 231 (2020) 394.